The Stabilization of Martensite in Cu-Zn-Al Shape Memory Alloys

G. SCARSBROOK, J. M. COOK, and W. M. STOBBS

The martensitic transformation temperature in shape memory alloys can be affected differently by aging above and below the transformation temperature. Under such circumstances the normally reversible transformation can be prevented and the martensite structure "stabilized". This effect has been studied using electron microscopy, differential scanning calorimetry, and mechanical testing. Evidence is given of an apparently martensitic high temperature transformation, and a careful comparison is made of the stabilized and unstabilized states of the alloy. Three possible models for stabilization are considered in the light of the results obtained, and it is concluded that no single mechanism can be responsible for all the phenomena observed.

I. INTRODUCTION

Cu-based shape memory alloys are susceptible to low temperature aging effects which can radically alter their transformation behavior, and may limit their reliability as temperature sensitive components in devices such as thermostats.

Both the parent and the martensitic phase are susceptible to aging effects. As has been recently reviewed,[1] changes in M_s which can be reversible (*e.g.*, References 2 to 5) result either from aging treatments above M_s or from subjecting the alloy to different quench temperatures above M_s. In Cu-Zn-Al these effects, which are accelerated by a high concentration of quenched-in vacancies, can be modeled on changes in the configurational order of the parent phase altering the relative free energies of the parent and martensite.[5-8]

Here we are concerned with the 'stabilizing' effect of aging Cu-Zn-Al in the martensitic state.[1,3] Such treatments, which are again accelerated by a high vacancy concentration, can raise A_s sufficiently to alter the normal transformation sequence to ordered cubic β_1.[4,9] If, however, the parent phase is formed, subsequent thermal cycles show normal transformation temperatures unless the alloy is again aged in the martensitic state.[9,10,11]

An apparently related effect has been commercially applied for the convenient storage of SME pipeline couplings made of Cu-Zn-Si.[12] This alloy will remain martensitic if heated slowly to a temperature T_c above the 'normal' A_f, but if it is then cooled and rapidly heated to above T_c, it transforms to parent phase at a temperature near T_c.

Various mechanisms have been proposed for martensite stabilization. These are:

(i) martensite boundary pinning by vacancies or vacancy clusters;[10,11]
(ii) the lowering of the martensite free energy by changes in the configurational order of the martensite, assisted by a high quenched-in vacancy population;[9] and
(iii) the inhibition of the normal transformation either by changes in the nature of the fault structure of the martensite, or by the formation of localized regions of the stable α phase.[13,14]

G. SCARSBROOK and W. M. STOBBS are with the Department of Metallurgy and Materials Science, University of Cambridge, England. J. M. COOK, formerly with the Department of Metallurgy and Materials Science, University of Cambridge, England, is now with Schlumberger Cambridge Research, Cambridge, England.

Manuscript submitted January 23, 1984.

Here we describe the results of further experiments designed to characterize the stabilization effect in a Cu-Zn-Al alloy (Section III). We compare the structure and order of the stabilized and unstabilized martensite (Section IV), give evidence of a high temperature martensitic transformation in stabilized material (Section V), and finally discuss the extent to which our results clarify the mechanism(s) of the stabilization process.

II. EXPERIMENTAL DETAILS

Three alloys, chosen to demonstrate different aspects of the stabilization phenomena, were supplied by Delta Memory Metal Ltd. (Ipswich, England) with compositions:

Alloy	Cu	Zn	Al	(At. Pct)
1	67.0	24.2	8.8	
2	67.8	23.2	9.0	
3	69.8	14.9	15.3	

All specimens were solution treated in the β-phase field at 1123 K, in air, and water quenched. Aging treatments were carried out in water or oil baths, and the martensite -β_1 transformation characterized for each treatment by DSC, using a Dupont 990 Thermal Analyser at a heating rate of 20 K per minute. Changes in microstructure were examined by electron microscopy using a Philips EM400ST microscope. Foils of material aged at a low temperature (<450 K) were thinned by twin jet electropolishing in a 25 pct nitric acid/10 pct glycerol/methanol solution at 14 V and room temperature, while material aged at higher temperatures was polished at lower temperatures (~240 K) and higher voltages (~25 V).

The tensile properties of stabilized and unstabilized martensite were compared using an Instron 8000 servo hydraulic machine with a clip-on extensometer. The specimens had a gauge-length diameter of 5 mm, in an attempt to minimize the effects of the alloy's characteristically large grain size (0.5 to 1.0 mm). Vickers hardness measurements were also made.

III. CHARACTERIZATION OF STABILIZATION

Different degrees of martensite stabilization are shown in Figure 1 by DSC traces for alloys 1 and 2. When alloy 1 is quenched from 1123 K to room temperature and aged at this temperature for 24 hours, the reverse transformation

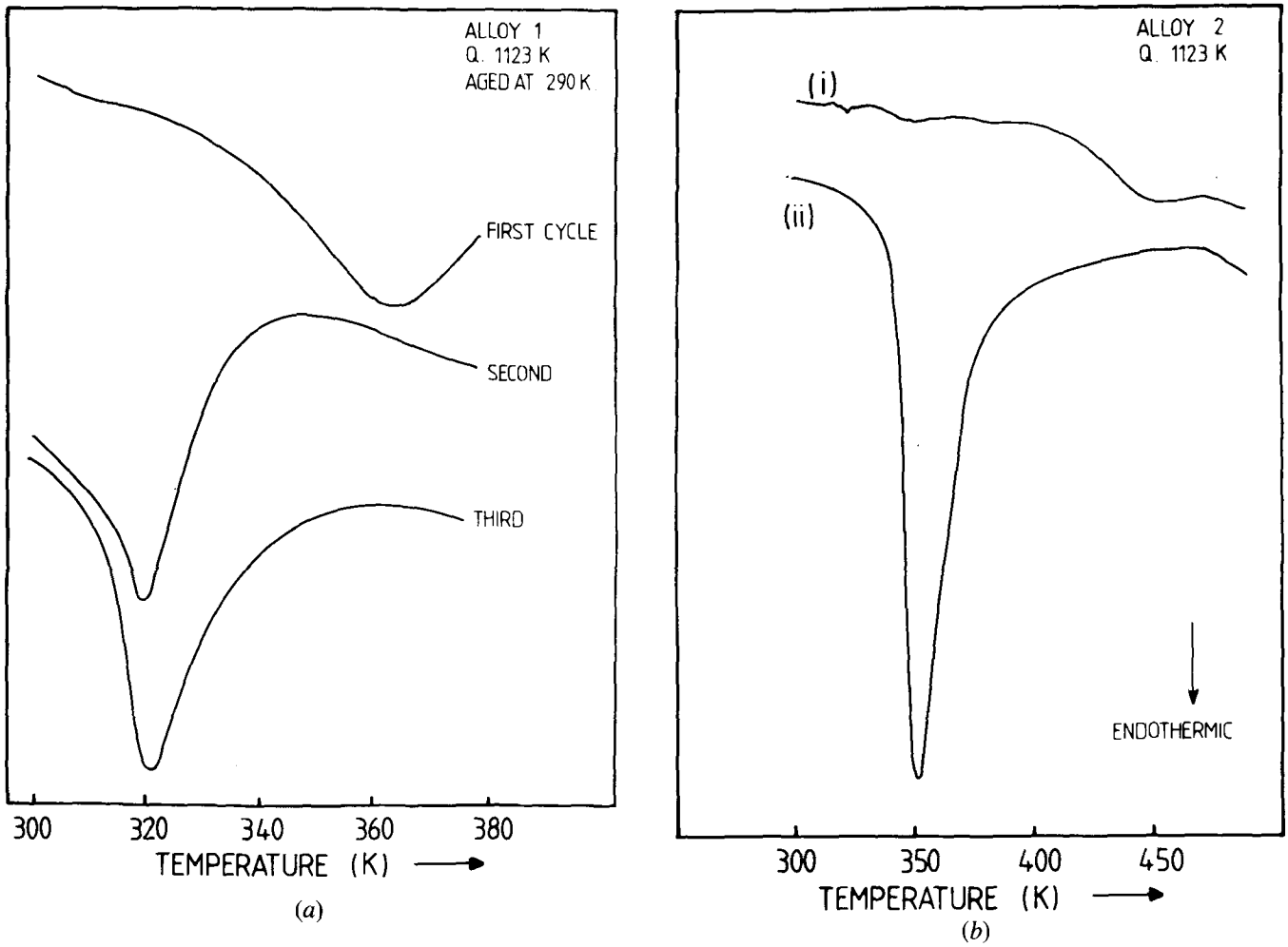

Fig. 1—DSC traces of alloys 1 and 2. (*a*) The first three heating curves of an alloy 1 specimen after quenching to room temperature and aging there for 24 h. (*b*) Alloy 2 quenched to room temperature and subsequently either held at this temperature for 24 h (curve (i)), or immediately up-quenched to 360 K for 1 h, then held at room temperature for 24 h (curve (ii)).

in the first heating cycle occurs over a broad range of temperature centered at 365 K (Figure 1(a)). Subsequent heating cycles exhibit much sharper transformation peaks, centered at a temperature of 321 K. Alloy 2, when treated similarly to alloy 1, shows no evidence of bulk transformation to the parent phase (Figure 1(*b*), curve (i)). The indication of a weak endothermic reaction at 450 K may be associated with the formation of the parent phase in a fine lamellar morphology as is discussed in Section V. Curve (ii) in Figure 1(b) is for alloy 2 quenched to room temperature, immediately up-quenched to 360 K and aged there for 1 hour, then quenched again to room temperature and aged there for 24 hours. The alloy then shows a normal, reversible, and repeatable martensitic transformation with an endothermic peak centered at 350 K. The important difference between these two heat treatments is that the latter one entails time spent in the parent phase field immediately after the quench from 1123 K.

Alloy 3 exhibits similar behavior to alloy 2 after similar heat treatments. The martensite transforms reversibly to parent phase with $A_s \sim 360$ K if after solution treatment it is either air-cooled, or quenched to temperatures above 370 K, or quenched to room temperature and immediately up-quenched to 370 K. However, as for alloy 2, if it is quenched directly into the martensitic phase field and either aged in the martensitic state or heated slowly (20 K per minute), the martensite becomes stabilized and will not transform to the parent phase in the normal manner.

It would thus appear that if a Cu-Zn-Al alloy is quenched into the martensitic phase field, changes occur which raise the reverse transformation temperature to a degree that is partially dependent on alloy composition. If, however, the alloy is held in the parent phase field for an appreciable period, then the susceptibility to stabilization is reduced and any stabilization that has previously occurred is removed.

The kinetics of the changes occurring in the martensitic phase during stabilization have been examined for alloy 3. This was accomplished by measuring the endothermic peak area of DSC heating traces (giving the proportion of reversibly transforming martensite) taken from specimens heat treated as follows:

(i) solution treatment for 6 minutes at 1123 K;
(ii) quench to one of five aging temperatures: (a) 273 K, (b) 293 K, (c) 297 K, (d) 320 K, (e) 328 K, followed by a hold at this aging temperature for one of a sequence of times;
(iii) up-quench into boiling water (373 K) for 10 minutes, both to transform the remaining unstabilized martensite to parent phase and to remove the susceptibility of this fraction of the material to subsequent stabilization; and
(iv) quench to 273 K.

The specimens thus obtained contained, at room temperature, different volume fractions of stabilized and of unstabilized martensite as a function of aging time and temperature (Figure 2). From this figure it is clear that the stabilization is more rapid at higher temperatures. An Arrhenius plot of the time for 50 pct stabilization against temperature (Figure 3) indicates that the process is thermally activated with a single activation energy of 87.3 ± 2.5 kJ mol^{-1}.

The stabilization process as a function of aging could also be followed by measurements of the Vickers hardness, and results for two specimens of alloy 3 aged at 284 K and 305 K after a down-quench from 1123 K are shown in Figure 4. The hardness of the alloy rises from ~158 V_H in the unstabilized state to ~180 V_H in the stabilized state. These two sets of data are consistent with the activation energy derived above, although there is considerable scatter which may be the result of inhomogeneity in the stabilization process.

The tensile properties of the stabilized martensite were compared with those of the normal reversibly transforming martensite for alloy 2. Stress-strain curves for the material

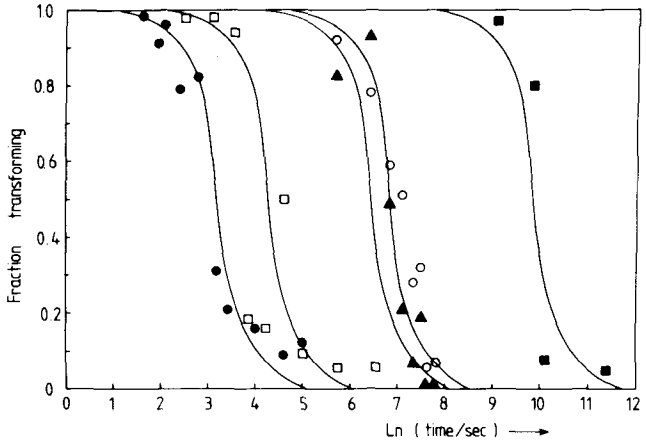

Fig. 2—The kinetics of stabilization of alloy 3. Each set of points shows the fraction of martensite reversibly transforming as a function of the aging time at each of the following temperatures: (*a*) 273 K (■), (*b*) 293 K (○), (*c*) 297 K (▲), (*d*) 320 K (□), and (*e*) 328 K (●) (see text). The curves drawn are of the same shape and fitted to each set of points by a simple regression technique.

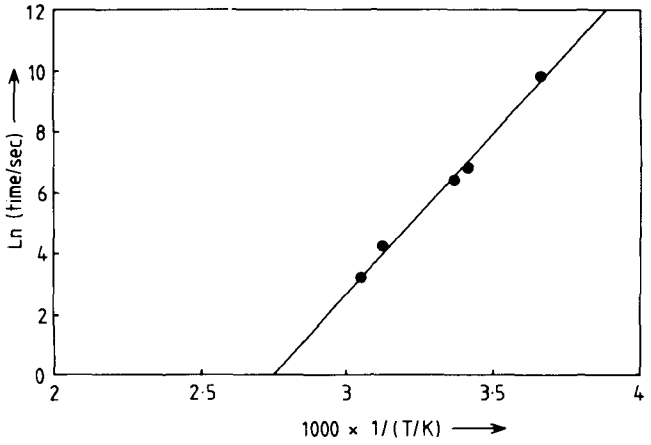

Fig. 3—Arrhenius plot of the time for 50 pct stabilization derived from the results in Fig. 2. The derived activation energy is 87.3 ± 2.5 kJ mol^{-1}.

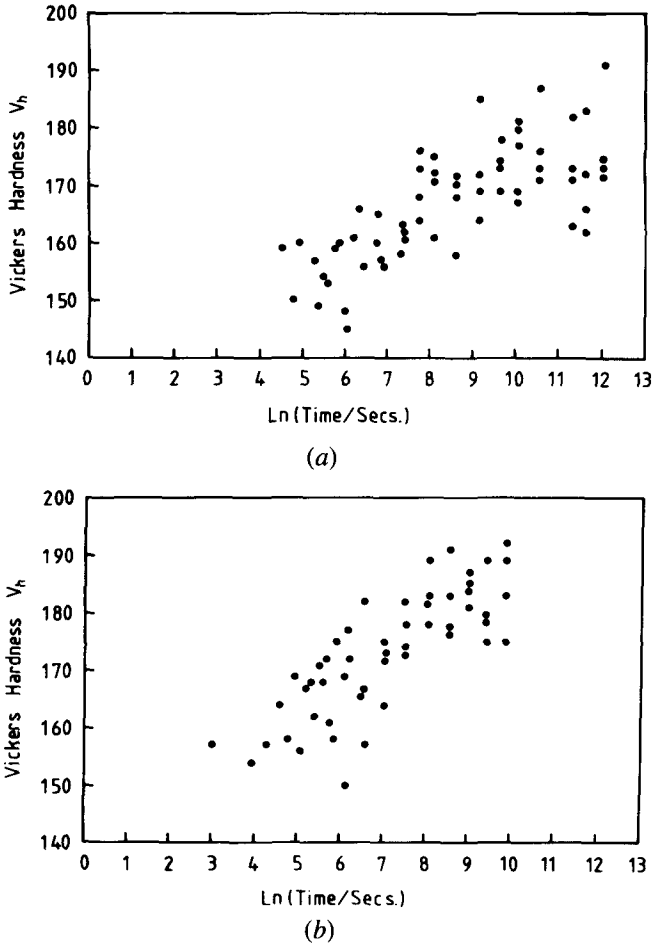

Fig. 4—Vickers hardness measurements for alloy 3 as a function of aging time at 284 K (*a*) and 305 K (*b*) after an initial quench from 1123 K.

in each state are shown in Figure 5, and it is immediately apparent that the stabilized alloy is markedly more difficult to deform than the normal martensite, though the work-hardening rates for each are remarkably similar. Neither

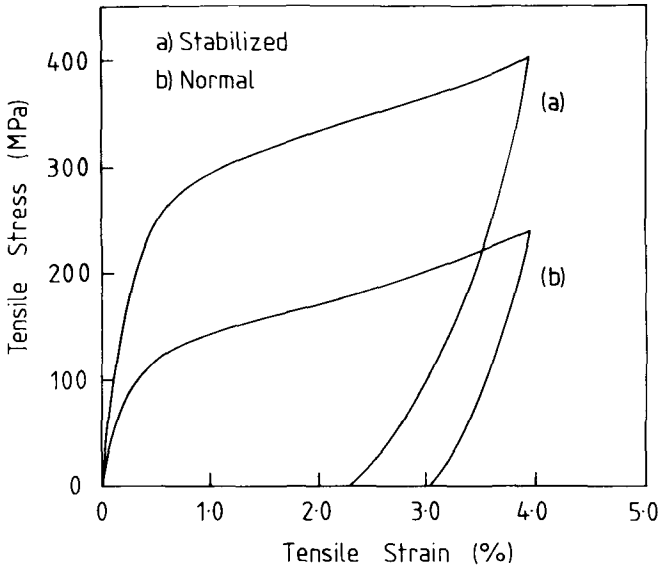

Fig. 5—Tensile stress-strain curves for polycrystalline martensitic alloy 2 in (*a*) the stabilized state and (*b*) the normally transforming state.

curve exhibits a yield drop despite the testing machine being sufficiently hard to exhibit such an effect, but the stabilized material undergoes a much larger reverse flow on unloading than the normal martensite. Similar effects have been observed by Janssen *et al.*[11]

IV. MARTENSITE STRUCTURE AND ORDER

In our previously reported work on alloy 3[9] using X-ray powder photography, we found no differences between the structures of stabilized and unstabilized martensite. The structure was found to be M18R, as for similar alloys.[15] Comparison of experimental line positions and intensities with values calculated for a fully-ordered M18R alloy of this composition gives the following lattice parameters:

$$a = 0.4408 \text{ nm},$$
$$b = 0.5308 \text{ nm},$$
$$c = 3.819 \text{ nm},$$
$$\beta = 88.70°.$$

However, because of the densely populated reciprocal lattice of the martensite and the large grain size of the alloy, powder photographs are not suitable for the detection of differences between the states of order of the two types of martensite. We have therefore used a vertical diffractometer method, with a much larger specimen in an attempt to examine any differences in the degree of order of the stabilized and unstabilized martensites by comparisons of the intensities of superlattice reflections in the two materials. While both normal and stabilized martensite do exhibit superlattice reflections at the positions expected given the inheritance of DO_3 order from the parent phase, variations in peak intensity from specimen to specimen precluded any comparison being made of the degree of order. More interestingly, both normal and stabilized material showed marked variability in the lattice reflection positions by up to 1 pct. This is far too large a figure to be explained by any normal inhomogeneous elastic stress fields present in the material which would in any case lead to more line broadening than is observed. While it remains possible that the structure has inherent variability, our diffractometer results were obtained from near the surface of rolled material whereas our powder camera results were taken from heavily electropolished rod. Given, however, that no consistent differences were observed between the stabilized and unstabilized material, the structure analysis has not been taken further.

Comparisons of the state of order of the normal and stabilized martensite were also attempted using electron microscopy. Consistently with the X-ray results, both materials exhibited superlattice reflections indicating the inheritance of the DO_3 parent phase superlattice. Two kinds of antiphase domain (APD) boundary can thus be examined: one is imaged using the reflections which would occur if the parent phase had B2 order only, the other using the additional reflections which arise from the DO_3-derived superlattice. The APD size was found to depend on the temperature of the quenching bath. Figure 6, from a specimen of alloy 3 quenched to 400 K and thus containing normal martensite, shows a $[\bar{1}10]$ zone axis pattern with rows of B2- and DO_3-derived superlattice reflections, together with dark-field images of the APD boundaries, formed from each type of spot. Figure 7 shows the symmetry-related [110] diffraction

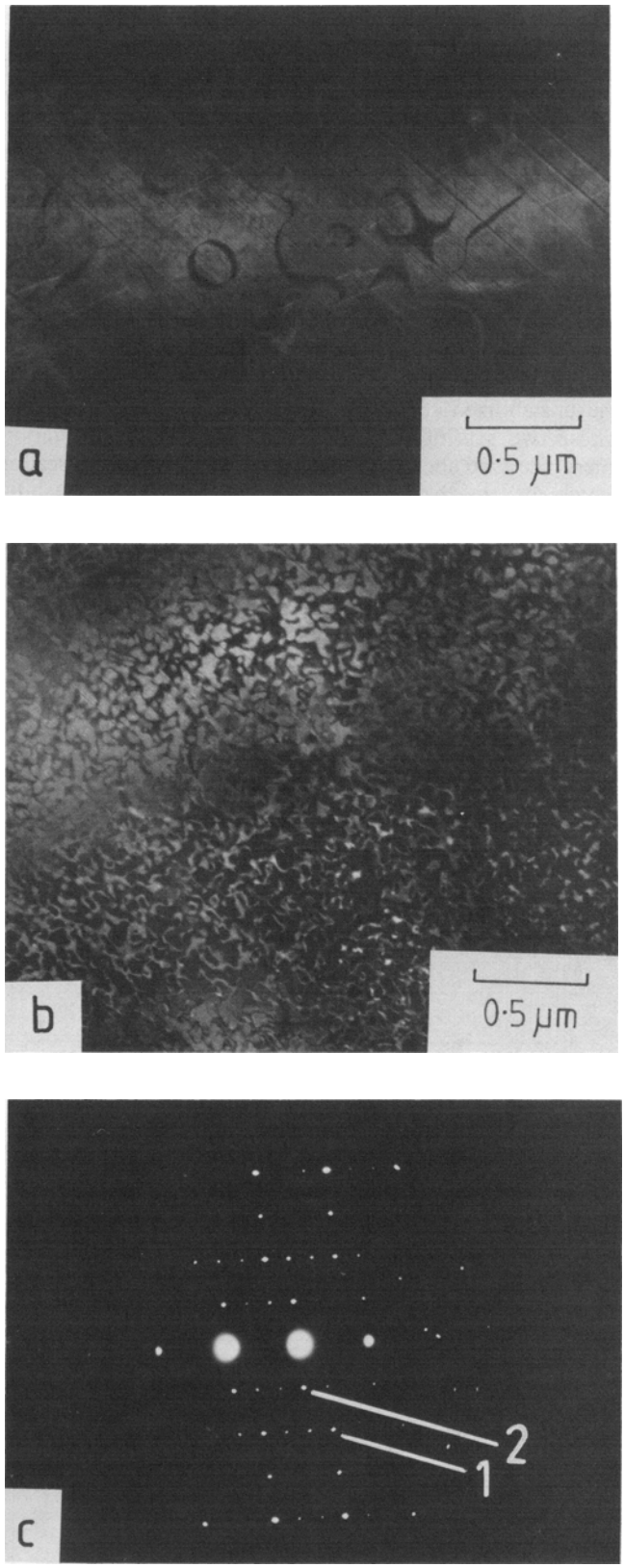

Fig. 6—Alloy 3 quenched to 400 K and thus unstabilized. (*a*) Dark-field transmission electron micrograph using a B2 order reflection as marked by (1) in the diffraction pattern (c). (*b*) Dark-field transmission electron micrograph of the same area as shown in (a) using a DO_3 order reflection as marked by (2) in the diffraction pattern (c). (*c*) Electron diffraction pattern of the area in (a) and (b) with beam direction $[\bar{1}10]$, the order reflections used for (a) and (b) being marked (1) and (2), respectively. The B2 APD size is ~1 μm, and the DO_3 APD size is ~0.1 μm.

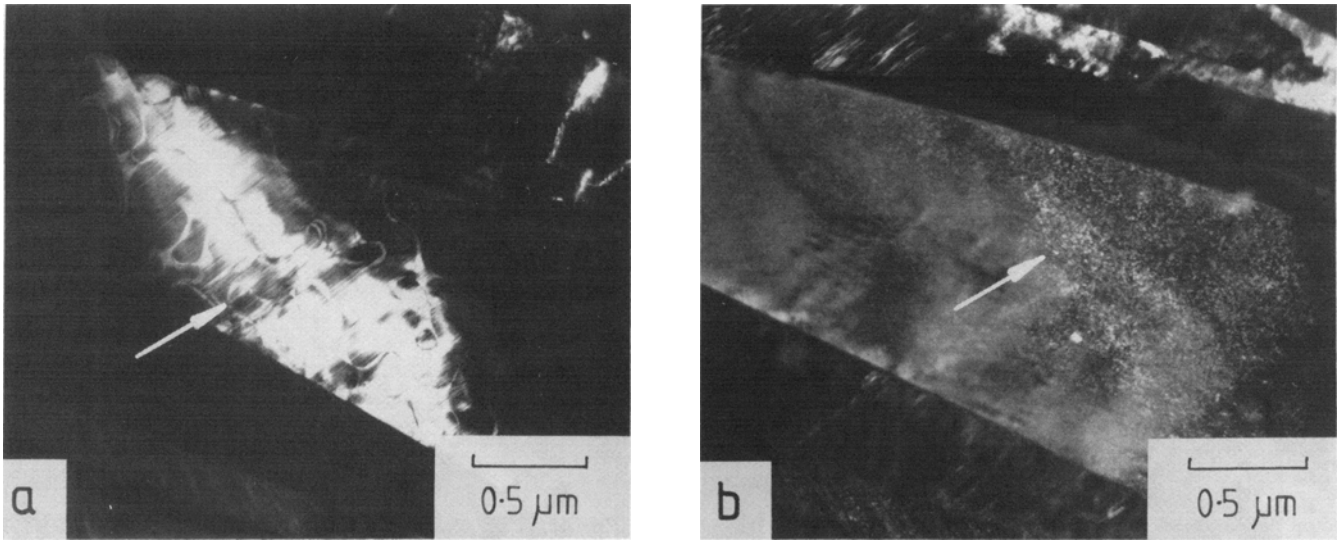

Fig. 7—Alloy 3 quenched to 273 K and thus stabilized. (*a*) Dark-field transmission electron micrograph using a B2 order reflection as marked by (1) in the diffraction pattern (c). (*b*) Dark-field transmission electron micrograph of the same area as shown in (a) using a DO_3 order reflection as marked by (2) in the diffraction pattern (c). (*c*) Electron diffraction pattern of the area in (a) and (b) with beam direction [110], the order reflections used for (a) and (b) being marked (1) and (2), respectively. The B2 APD size is ~0.4 μm, and the DO_3 APD size is ~20 nm. (In both (a) and (b) the respective regions showing B2 and DO_3 APD's are marked in the centrally located martensite variant. Intensity in other variants derives from necessarily included matrix reflections from these regions.)

pattern and image pair for a specimen quenched to 273 K and thus in the stabilized state. It may be seen that the APD size is considerably smaller in this stabilized martensite than in the working alloy in Figure 6. It is not, however, a small APD size which causes stabilization in this alloy since if the material quenched to 273 K is immediately up-quenched to 400 K, then martensite formed on subsequent cooling is in the working state but shows APD sizes (Figure 8) similar to those found in the stabilized martensite. It remains possible that the working and stabilized martensites differ in the degree of order within APD's, but this is difficult to assess using electron microscopy.

The variability of the structures of both the normal and stabilized martensite, as determined by X-ray techniques, could also have its origin in differences in the relative numbers of the various types of stacking fault which the martensite can contain.[13] Faults involving the removal or insertion of a plane from the structure, which then cannot be removed by a simple shear, could inhibit the normal martensitic transformation, and faults of this type have been observed in the stabilized material.[14] Further attempts were therefore made to see if there are differences in the fault populations in the two different martensites. At the high resolution (0.2 nm), low specimen thickness and very precise specimen alignment necessary for a full structure determination of the faults, statistical analysis of their relative frequencies has proved impracticable. We have, however, found that lower resolution images can exhibit sufficiently reliable lattice fringe displacements across both the two classes of sequence fault and shear faults for these to be distinguished. Preliminary results indicate that there are no substantial differences in the relative population of the different classes of sequence fault in the normal and stabilized material and that few simple shear faults are ever present.[16]

V. THE TRANSFORMATION MORPHOLOGIES ON HEATING

The normal unstabilized martensite in alloy 3 transforms to the parent phase at ~360 K. The transformation can be observed optically, and shows the normal mode of transformation expected for this type of alloy. As heating proceeds individual martensitic plates and groups of variants shrink either smoothly or discontinuously.[8] Plate-shaped regions of the parent phase are also sometimes seen growing within a martensite plate (Figure 9).

The stabilized martensite in alloy 3 shows some endothermic activity above 520 K; this is similar to the behavior of alloy 2 shown in Figure 1(b). The microstructural

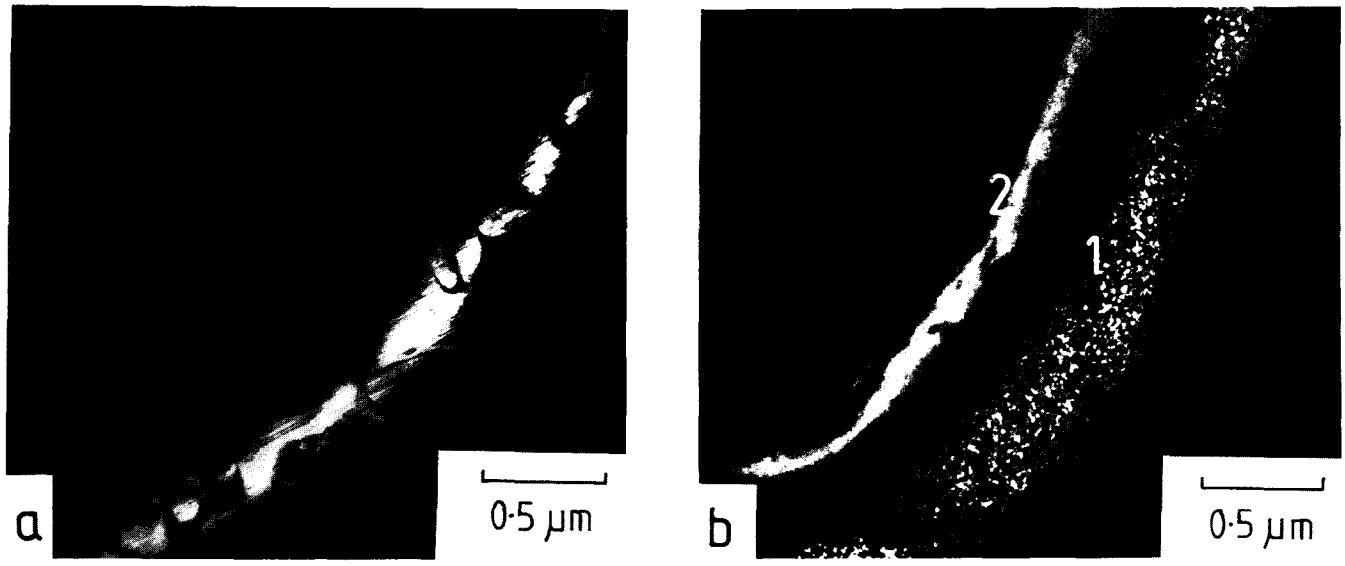

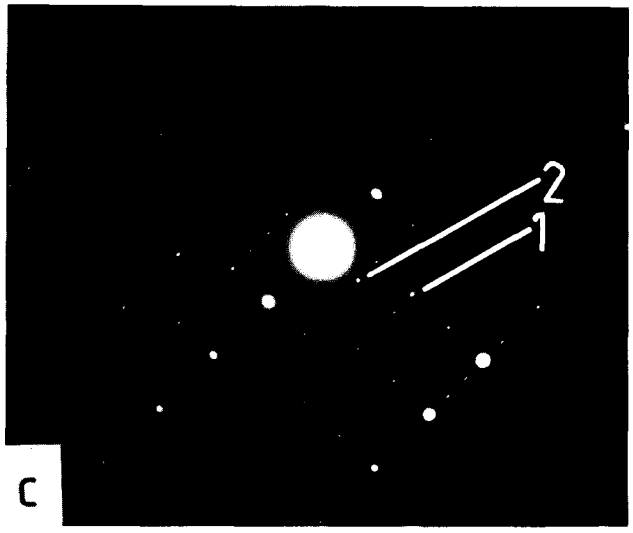

Fig. 8—Alloy 3 quenched to 273 K then immediately up-quenched to 400 K, and thus unstabilized. (*a*) Dark-field transmission electron micrograph using a B2 order reflection as marked by (1) in the diffraction pattern (c). (*b*) Dark-field transmission electron micrograph of the same area as shown in (a) using a DO_3 order reflection as marked by (2) in the diffraction pattern (c). (*c*) Electron diffraction pattern of the area in (a) and (b) with beam direction $[\bar{1}10]$, the order reflections used for (a) and (b) being marked (1) and (2), respectively. The B2 APD size is 0.5 μm, and the DO_3 domain size is ~30 nm. (Note that in (b) the aperture position was such as to include the edge of a B2 order reflection resulting in the image showing both the DO_3 domain structure at (1) and more weakly the B2 structure at (2).)

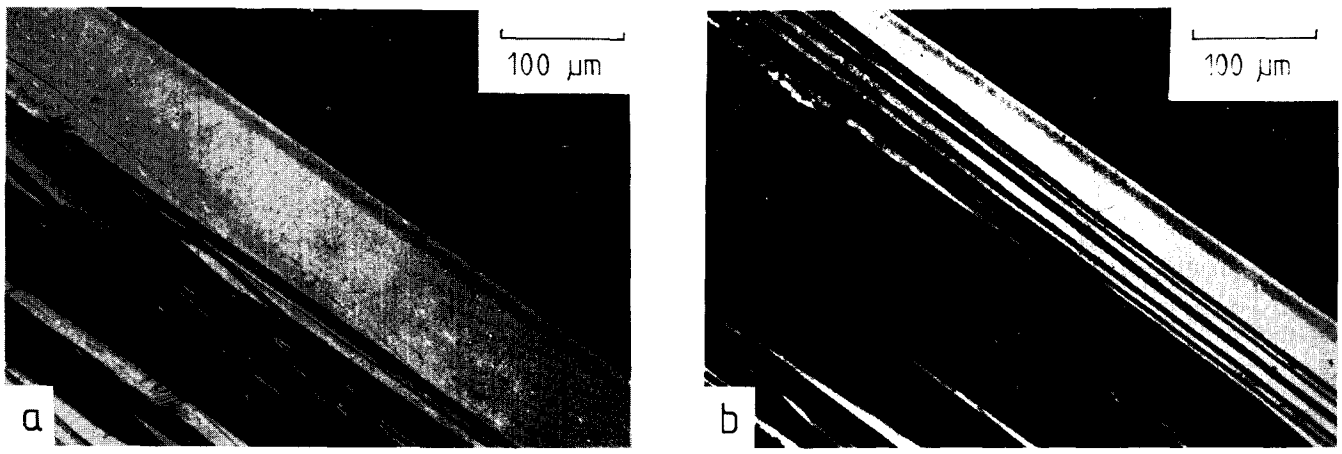

Fig. 9—Polarized light optical micrographs of a large martensite plate before (*a*) and during (*b*) heating through the reverse transformation. The dark bands in the central otherwise light colored plate in (b) are of parent phase, formed by the production of new boundaries rather than by the movement of existing ones.

changes associated with this thermal activity were examined for alloy 3 by the TEM of specimens of stabilized martensite aged at 570 K for 75 minutes. Most regions of this material were shown to be a modified form of the M18R martensite, with $a = 0.448$ nm, $b = 0.517$ nm, $c = 3.82$ nm, and $\beta = 90°$. (This martensite identification replaces the Z_α, Z_β characterization previously reported.[9]) Some martensite plates had reverted as a whole to the β_1 phase, in a morphology we will call "bulk β_1" to distinguish it from the "normal" parent phase as in unaged material. Many of the modified martensite regions contained fine lamellae which were also shown to be ordered cubic and will be called "lamellar β_1". These lamellae were typically 10 to 30 nm thick, but tapered toward martensite variant boundaries. The 570 K aged material also contained the cubic γ phase ($a = 0.89$ nm) at some grain and intervariant boundaries, with a spheroidal or rosette morphology.

Figure 10(a) shows a typical example of this microstructure, with two martensite plates separated by bulk β_1. One plate of martensite (Figure 10(b)) contains tapered lamellar β_1 (Figure 10(c)), and the bulk β_1 exhibits "tweed" related contrast commonly found in beta-brass-type phases. Figure 10(d) is a diffraction pattern of the bulk β_1/martensite + lamellar β_1 boundary, with beam direction $[\bar{8}0\bar{1}]_M$* and $[00\bar{1}]_{\beta_1}$. The orientation relationships are approximately

$\{110\}_{\text{bulk}}$ parallel to $(\bar{1}\ 2\ 8)_M$
$\{110\}_{\text{lamellar}}$ parallel to $(1\ 2\ \bar{8})_M$

These two orientation relationships are crystallographically identical, being related by the diad axis of the martensite structure, which suggests that both types of β_1 phase are produced by a martensitic mechanism. This idea is supported both by the tapered shape of the lamellae, which is indicative of a shape change during the transformation, and by the observation of the shear displacement of the stacking faults in the martensite matrix by the β_1 lamellae (Figure 11).

The habit planes of both bulk and lamellar β_1 with respect to the martensite lattice were determined approximately using TEM by tilting the martensite/β_1 boundary about $(0018)_M$, until the projected boundary width was minimized. Both habit planes were found to be of the form $\{\bar{1}, 1.3, 4.25\}_M$ [*i.e.*, $(\bar{1}, 1.3, 4.25)$ or $(\bar{1}, \overline{1.3}, 4.25)$], lending further support to the idea that the lamellar β_1 is formed by a martensitic mechanism. As can be seen from Figure 10(a), the bulk β_1 is formed with one of the above habit planes, the lamellar β_1 with the other, and each habit plane is close to ($\sim 13°$ from) the particular $\{\bar{1}28\}_M$ normal that is unrotated during the transformation.

Related microstructures have been observed in other alloys. In Cu-Al,[17] tapered β_1 lamellae are found after aging thin foils of martensite; it is not clear whether or not this is the only morphology seen. In Cu-Zn-Ga[18] two morphologies of precipitate have been found (within variants and at boundaries), but the precipitates in this case were of the γ_1 phase.

To summarize these results, it would appear that both unstabilized and stabilized martensite can revert to the β_1 phase on heating by a martensitic mechanism. When the unstabilized martensite reverts to β_1 it does so by plate shrinkage with an identical habit plane to that seen for the transformation on cooling. The stabilized martensite reverts at a higher temperature when the formation of γ phase indicates the possible importance of diffusion. The β_1 phase habit plane exhibited in this case is not restricted to that of the parent-to-martensite transformation, but can also be the plane related to it by the diad symmetry of the martensite. This leads to two morphologies of parent β_1 phase, with different orientations.

*The subscript M denotes plane or direction indices referred to the M18R martensite lattice.

VI. DISCUSSION

Three possible reasons for martensite stabilization were described in Section I, and here we will discuss the extent to which our results can be used to choose among these possibilities.

A. *Pinning of Martensite Plate Boundaries*

In this mechanism, quenched-in excess vacancies may migrate to plate boundaries after the quench into the martensite phase field, pinning them and thus preventing their athermal motion during heating through the normal reverse transformation temperature.

Internal friction measurements in similar alloys after quenching[11] show a rapid increase in damping followed by a slower fall. The fall is consistent with the idea of the pinning of variant boundaries by vacancies, but the cause of the initial increase is not clear. A similar peaking effect has been seen in irradiated pure metals (*e.g.*, Reference 19) as well as in normally transforming Cu-Zn-Al martensite.[20]

Pinning of existing boundaries, however, cannot prevent the growth of parent phase with new boundaries within martensite plates (at a temperature close to A_s) as can occur in the normal reverse transformation (Figure 9). This suggests that if boundary pinning is the dominant mechanism of stabilization, any increase in A_s could only be of the order of A_s-A_f (unless stabilization also affects nucleation). Furthermore, the stress-strain curve of stabilized martensite does not show a yield drop as would be expected with strong pinning of variant boundaries (*cf.* dislocation motion in mild steel[21]). As essentially all the variant boundaries will be unpinned after 4 pct tensile strain (as in Figure 5), the stress should have fallen, by this strain, to the value required to deform an unstabilized specimen, even if a sharp yield drop were masked by the range of Schmid factors present or by non-uniform stabilization throughout the specimen. The stabilized martensite also shows greater strain reversal on unloading than does normal martensite, and since boundary pinning is a short-range phenomenon, it is unlikely to be directly responsible for this effect.

B. *Changes in the Configurational Order*

The product of martensitic transformation is not the stable phase of a system, so it would not be surprising if the martensite were to undergo further structural changes after its formation, ultimately producing the stable phases (in Cu-Zn-Al, fcc α-phase and cubic β_1) but initially moving to a local free energy minimum. This decrease in the free energy of the martensite will also raise the free energy of the

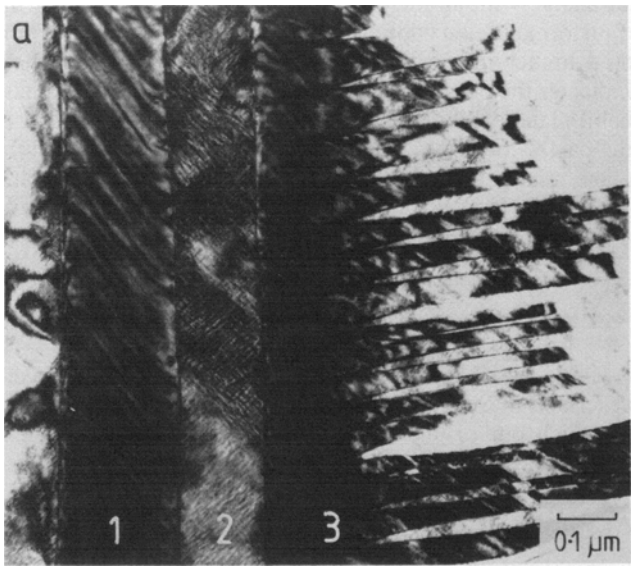

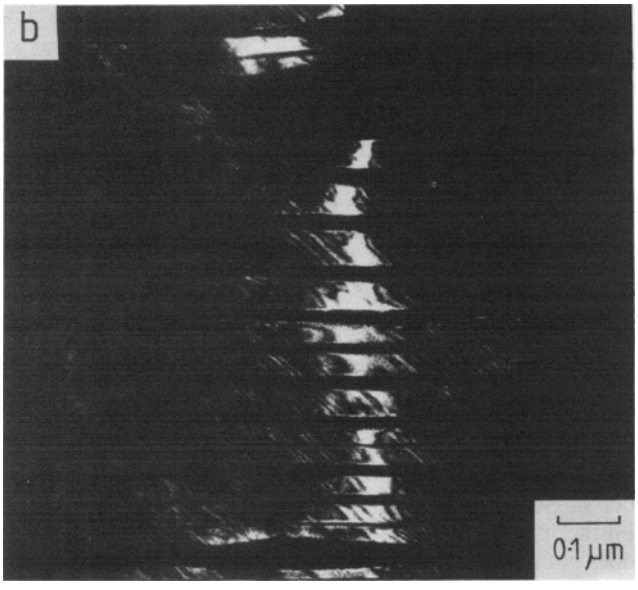

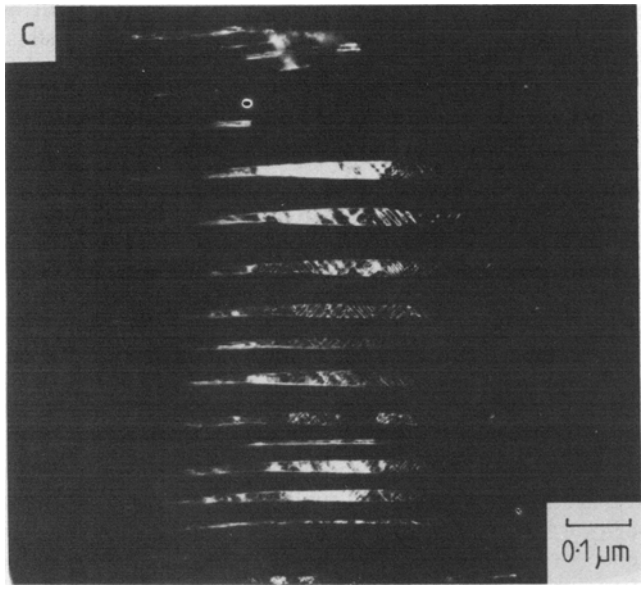

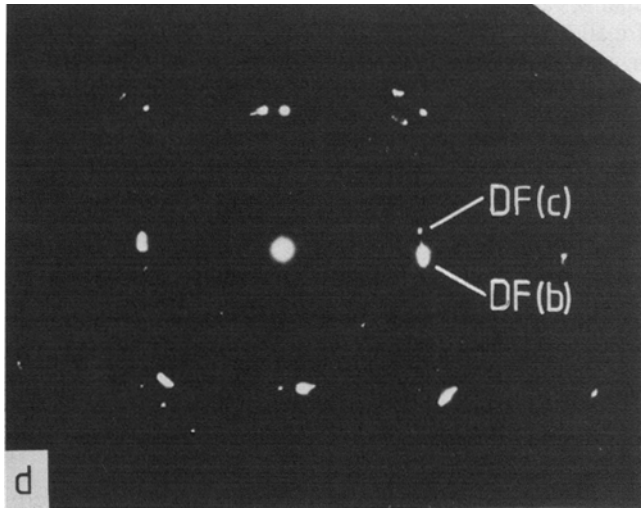

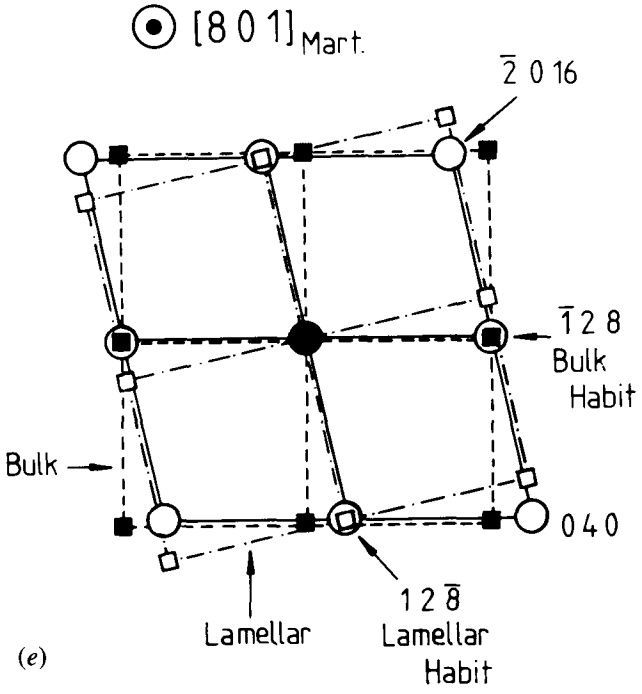

Fig. 10 — A region of the stabilized martensite in alloy 3 as aged at 570 K for 75 min. (*a*) Bright-field electron micrograph of the region as a whole. The martensite band (1) contains no "lamellar" β_1. The band (2) is "bulk" β_1, and the martensite variant (3) contains "lamellar" β_1 as imaged in dark field in (c). (*b*) Dark-field electron micrograph of the martensite variant (3) in (a) imaged using the β_1' reflection marked in the diffraction pattern of the area (d). Note the typical diagonal contrast associated with inclined martensite faulting. (*c*) Dark-field electron micrograph of the β_1 lamellae in region (3) of (a) imaged using the β_1 reflection marked in the diffraction pattern of the area (d). Note the strong cross-hatched contrast suggestive of an aging development from the normal "tweed" spinodal characteristic of the β_1 phase in this type of alloy. (*d*) Diffraction pattern of the area oriented with respect to the images (a), (b), and (c) and indexed with respect to the different phases imaged in (e). The beam is $[\bar{8}0\bar{1}]$ in the β_1' phase and $[00\bar{1}]$ in the β_1 bulk and lamellae phases. (*e*) An indexed diagram of the diffraction pattern (d). The key shows the $\{\bar{1}28\}$ planes which are close to the habit planes of bulk (■), and lamellar (□), β_1. The beam direction is $[\bar{8}0\bar{1}]_M$ and $[00\bar{1}]_{\beta_1}$.

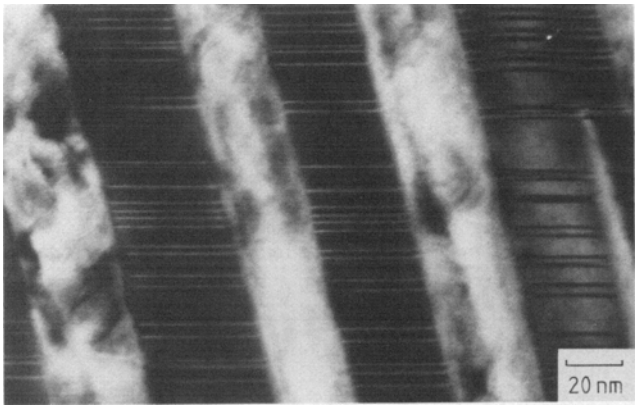

Fig. 11 — β_1 lamellae (light) in a stabilized and aged martensite plate. The horizontal lines in the martensite are stacking faults formed during the martensitic transformation, and their displacement by the β_1 lamellae is clear.

parent phase to which it could revert, and jointly these effects will raise the A_s temperature.

In this model for stabilization, the structural change expected is in the state of configurational order of the martensite. The superlattice that the martensite inherits from the parent phase may not be a local minimum free energy configuration for the martensite, but is produced because the transformation is diffusionless.

If diffusion is relatively fast after the transformation, as would be the case in the presence of a high supersaturation of quenched-in vacancies, the martensite may lower its free energy by reordering causing A_s to rise. If the material is transformed to the β_1 phase after only partial stabilization, the high diffusion rates and strong tendency to order in the parent phase, together with the remaining quenched-in vacancies, will allow the return of the β_1 phase to its equilibrium state of order. Rapid diffusion in the β_1 state then reduces the excess vacancy population, and on subsequent cooling the alloy transforms to the 'normal' reversible martensite with a state of order inherited from the β_1 phase. This state of order is again of relatively high energy, but in the absence of a high supersaturation of quenched-in vacancies there is no rapid way of lowering the energy.

This model of stabilization explains the thermal phenomena, and is consistent with the change in the monoclinic angle β which occurs during aging of stabilized martensite, which suggests a decrease in order. The rate-determining step of the stabilization process (as in the other approaches) is the motion of vacancies, and our measured activation energy of 87.3 kJ mole^{-1} (Figure 3) is thus not unreasonable.

The change in order that stabilizes the martensite can alter the symmetry of the martensite lattice. If this alteration is such that the motion of an intervariant boundary no longer reproduces the lattice that it moves through, but creates a new lattice, then there will be a restoring force on the boundary. Such a phenomenon has been observed in other alloys, for example Fe-Be.[22] This restoring force will increase the stress needed to deform the martensite and tend to remove applied strain on unloading, which is the behavior seen in stabilized martensite (Figure 5).

Even if the symmetry of the lattice is not changed by stabilization, the mechanical effects seen can result from changes in the short-range disorder present in the martensite. Rapacioli and Ahlers[6] show that there are disordered next-nearest-neighbor pairs in the parent phase which are transformed into one of two kinds of disordered pair in the martensite lattice, according to whether or not the line joining the disordered pair in the parent is parallel to the unique Bain axis of the transformation. These two kinds of disordered pair have different energies in the martensite, and this approach has been used to model the rubber-like effect in Cu-Zn-Al martensite by Ahlers *et al.*[23] In the particular case of $Al^{[IV]}Zn^{[III]}$ pairs (using the notation of Rapacioli and Ahlers) the lines joining the pairs in the parent are parallel to $\langle 100 \rangle$ directions, and so, since the Bain axis also lies along a $\langle 100 \rangle$ direction, twice as many of one kind of defect as the other will be produced in the martensite. This is not the equilibrium ratio, which is determined approximately by a Boltzmann distribution using the formation energies of the respective disordered pairs. During stabilization, the quenched-in vacancies allow this equilibrium ratio to be achieved. On subsequent transformation, during deformation, to another variant with a different Bain axis (such as occurs by motion of an intervariant boundary on $(114)_{9R}$ as described by Schroeder and Wayman,[24] the ratio of the numbers of the two kinds of defect must again depart from its equilibrium value, thus raising the free energy of the newly-formed variant. Equally, on transformation to the parent phase, both the related defects become a single type of defect with a higher energy, raising A_s.

It is not suggested that this is the principal or the only mechanism operating in Cu-Zn-Al stabilization, or that $Al^{IV}Zn^{III}$ disordered pairs are the dominant defects. However, in the absence of a more massive change in order, this kind of pair-defect restructuring is predicted by present models.

It should also be noted that the structure of an ordered Cu-Al martensite is modified by tempering;[25] a new long-period superlattice is produced, followed by annihilation of the stacking faults. This is a clear example of the tendency of Cu-based martensites to undergo structural modifications.

A model based on reordering does not appear to predict the formation of parent phase on the two related habit planes (Section V). This observation suggests that the transformation is inhibited at the original interface, as, for example, by vacancy pinning. 'Superheating' of the martensite could then lead to a chemical driving force sufficient to overcome the greater elastic energy associated with the formation of constrained thin β_1-phase lamellae. Furthermore, in normal working martensite, boundary misorientation would appear to be effective in reducing local stress fields. Figure 10 shows, however, that the growth of β_1 phase lamellae is inhibited near existing boundaries, suggesting that movement of the latter is inherently more difficult than growth of the lamellae. Since motion of the two types of cubic/martensite interface must be equally affected by any volume effect such as ordering, this again suggests some form of pinning of the existing boundary.

C. *Changes in the Fault Structure of the Martensite*

If quenched-in vacancies migrate and cluster on a single $(0018)_M$ plane in the martensite, they will form a stacking defect which cannot be produced by a single shear, since in the M18R lattice such a fault is distinct from a fault produced by the passage of a partial dislocation (which is not

the case in fcc). An example of such a stacking defect, compared to the perfect M18R lattice, is

A B′ C B′ C B C′ A C′ A B ..... Defect
A B′ C B′ C A′ C A′ B A′ B .... Perfect

Defects of this type, involving removal of a plane, and others involving an extra plane, have been identified in stabilized Cu-Zn-Al martensite by high resolution electron microscopy.[13,14] If such defects were formed by quenched-in vacancies after the martensitic transformation, they might be expected to inhibit the reverse transformation by imposing a friction stress on the martensite/parent boundary or by increasing the free energy of the resultant parent phase. However, since we have found no gross population differences of the various types of defect in the stabilized and unstabilized material, it would appear that mechanisms of this type are unimportant.[16]

VII. CONCLUSIONS

We have here discussed three possible mechanisms for the thermally activated process of stabilization found in Cu-Zn-Al. Each requires enhanced diffusion, and experimental evidence supports the idea that this is associated with a supersaturation of quenched-in vacancies in the martensite. The third model mentioned, that involving stacking faults which include insertion or removal of an extra plane, would appear, on our preliminary results, to be inapplicable. Neither of the other two models can alone explain the experimental data considered here. Presently it would appear necessary for a complete model to include both an interface friction component such as vacancy pinning, and a volume energy term such as that derived from reordering. Both these processes are likely to occur, and experimentally it may be difficult to study each in isolation.

ACKNOWLEDGMENTS

We are grateful to Delta Memory Metal Ltd. and INCRA for financial support and provision of materials, and to Professor R. W. K. Honeycombe FRS for the provision of laboratory facilities.

REFERENCES

1. D. P. Dunne and N. F. Kennon: *Metals Forum*, 1981, vol. 4, pp. 176-83.
2. N. F. Kennon: *Met. Sci. Journal*, 1972, vol. 6, pp. 64-66.
3. R. Rapacioli, M. Chandrasekaran, and L. Delaey: in *Shape Memory Effects in Alloys*, J. Perkins, ed., Toronto, Plenum, New York, NY, 1975, pp. 365-78.
4. N. F. Kennon, D. P. Dunne, and L. Middleton: *Metall. Trans. A*, 1982, vol. 13A, pp. 551-55.
5. J. M. Cook and L. M. Brown: *Scripta Metall.*, 1978, vol. 12, pp. 949-52.
6. R. Rapacioli and M. Ahlers: *Acta Metall.*, 1979, vol. 27, pp. 777-84.
7. D. Schofield and A. P. Miodownik: *Metals Technology*, April 1980, pp. 167-73.
8. J. M. Cook: Ph.D. Thesis, University of Cambridge, England, 1980.
9. G. Scarsbrook, J. M. Cook, and W. M. Stobbs: *ICOMAT 82*, L. Delaey and M. Chandrasekaran, eds., Leuven, 1982, pp. 703-08.
10. A. Arab and M. Ahlers: *ICOMAT 82*, L. Delaey and M. Chandrasekaran, eds., Leuven, 1982, pp. 709-14.
11. J. Janssen, J. Van Humbeeck, M. Chandrasekaran, N. Mwamba, and L. Delaey: *ICOMAT 82*, L. Delaey and M. Chandrasekaran, eds., Leuven, 1982, pp. 639-45.
12. Raychem Corporation, French Patent No. 2301604.
13. W. M. Stobbs: *J. Microscopy*, 1983, vol. 129, pp. 307-14.
14. J. M. Cook, M. A. O'Keefe, D. J. Smith, and W. M. Stobbs: *J. Microscopy*, 1983, vol. 129, p. 295.
15. S. Chakravorty and C. M. Wayman: *Acta Metall.*, 1977, vol. 25, pp. 989-1000.
16. J. M. Cook and W. M. Stobbs: INCRA project No. 340, final report, 1983.
17. S. Kajiwara and Z. Nishiyama: *Jap. J. Appl. Phys.*, 1964, vol. 3, pp. 749-56.
18. L. Delaey and H. Warlimont: *Zeit. Met.*, 1966, vol. 57, pp. 793-803.
19. J. A. Caro and M. Mondino: *J. Appl. Physics*, 1981, vol. 52, pp. 7147-54.
20. J. Van Humbeeck and L. Delaey: *ICOMAT 82*, L. Delaey and M. Chandrasekaran, eds., Leuven, 1982, pp. 691-95.
21. R. E. Smallman: *Modern Physical Metallurgy*, 3rd ed., Butterworths, 1970, p. 315.
22. M. L. Green and M. Cohen: *Acta Metall.*, 1979, vol. 27, pp. 1523-38.
23. M. Ahlers, G. Barcelo, and R. Rapacioli: *Scripta Metall.*, 1978, vol. 12, pp. 1075-78.
24. T. A. Schroeder and C. M. Wayman: *Acta Metall.*, 1977, vol. 25, pp. 1375-91.
25. I. Lefever and L. Delaey: *Acta Metall.*, 1972, vol. 20, pp. 797-802.